PCCP

PAPER

View Article Online
View Journal | View Issue

Cite this: *Phys. Chem. Chem. Phys.*, 2019, **21**, 4200

Stability and flexibility of heterometallic formate perovskites with the dimethylammonium cation: pressure-induced phase transitions†

Maciej Ptak, *[a] Katrine Louise Svane, ‡[b] Aron Walsh [cd] and Waldeci Paraguassu [e]

Received 19th November 2018,
Accepted 5th February 2019

DOI: 10.1039/c8cp07131d

rsc.li/pccp

We report the high-pressure properties of two heterometallic perovskite-type metal–organic frameworks (MOFs) templated by dimethylammonium ($NH_2(CH_3)_2$, DMA^+) with the general formula $[DMA]M^{I}_{0.5}Cr^{III}_{0.5}(HCOO)_3$, where M^I = Na^+ (DMANaCr) and K^+ (DMAKCr). The high-pressure Raman scattering studies show crystal instabilities in the 4.0–4.4 GPa and 2.0–2.5 GPa ranges for DMANaCr and DMAKCr, respectively. The mechanism is similar in the two compounds and involves strong deformation of the metal-formate framework, especially pronounced for the subnetwork of CrO_6 octahedra, accompanied by substantial compressibility of the DMA^+ cations. Comparison with previous high-pressure Raman studies of sodium-chromium heterometallic MOFs show that the stability depends on the templated cation and increases as follows: ammonium < imidazolium < DMA^+. Density functional theory (DFT) calculations are performed to get a better understanding of the structural properties leading to the existence of phase transitions. We calculate the energy of the hydrogen bonds (HBs) between the DMA^+ cation and the metal formate cage, revealing a stronger interaction in the DMAKCr compound due to a HB arrangement that primarily involves the energetically preferred bonding to KO_6 octahedra. This material however also has a smaller structural tolerance factor (TF) and a higher vibrational entropy than DMANaCr. This indicates a more flexible crystal structure, explaining the lower phase transition pressure, as well as the previously observed phase transition at 190 K, which is absent in the DMANaCr compound. The DFT high-pressure simulations show the largest contraction to be along the trigonal axis, leading to a minimal distortion of the HBs formed between the DMA^+ cations and the metal-formate sublattice.

1. Introduction

The heterometallic formate metal–organic frameworks (MOFs) with perovskite-type structure and general formula $[A]M^{I}_{0.5}M^{III}_{0.5}(HCOO)_3$ (A = protonated amine, M^I = Na^+, K^+ and M^{III} = Al^{3+}, Cr^{3+}, Fe^{3+}) have attracted a lot of attention due to their interesting properties, including efficient luminescence,[1–5] ferroelectricity[3,6] or ferroelasticity.[7] The increasing number of analogues with different protonated amines leads to better understanding of the physical phenomena associated with the occurrence or absence of phase transitions.[1–8] Previous studies of this group of compounds have showed that the replacement of the protonated amine or the metal ion in the crystal lattice can dramatically change the properties and/or the stability of the material.[1–8] Therefore, the understanding of factors influencing the stability (the energy of the hydrogen bonds (HBs), their arrangement, the metal-formate framework flexibility, *etc.*) is an important task in order to realize the prospective applications and design materials with desired physicochemical properties.

The first MOF with the dimethylammonium cation (DMA^+) and metal-formate framework composed of alkali and transition metal ions, DMANaFe, was discovered in 2014 by Mączka *et al.*[7] This MOF adopts trigonal $R\bar{3}$ symmetry with the DMA^+ cations dynamically disordered into tree equivalent positions. It has been shown that the dielectric anomaly observed at 167 K is related to the first-order structural phase transition to

[a] *Institute of Low Temperature and Structure Research, Polish Academy of Sciences, Wrocław, Poland. E-mail: m.ptak@intibs.pl*
[b] *Department of Chemistry, University of Bath, Bath, UK*
[c] *Department of Materials, Imperial College London, London, UK*
[d] *Department of Materials Science and Engineering, Yonsei University, Seoul, Korea*
[e] *Faculty of Physics, Federal University of Para, Belem, Brazil*

† Electronic supplementary information (ESI) available: Fig. S1: XRD patterns; Tables S1–S4: experimental XRD and calculated unit cell parameters, hydrogen bonds parameters, calculated C–O bond lengths and calculated pressure dependence on the DMANaCr structure. DFT optimised structures and output files from the phonon calculations are available from https://doi.org/10.5281/zenodo.1474193. See DOI: 10.1039/c8cp07131d

‡ Current address: Department of Energy Conversion and Storage, Technical University of Denmark, Kgs. Lyngby, Denmark.

triclinic $P\bar{1}$ symmetry mainly driven by the ordering of DMA^+ cations and accompanied by the distortion of the metal-formate framework.[7] Further research has shown that the substitution of Fe^{3+} by Cr^{3+} ions completely suppresses this phase transformation, *i.e.* the decrease of temperature of DMANaCr leads only to the freezing out of DMA^+ rotations around the trigonal axis.[1] However, an interesting feature has been observed when relatively small Na^+ ions were replaced by larger K^+ ions.[2] The DMAKCr compound adopts trigonal symmetry (space group $R\bar{3}$) with the DMA^+ cations disordered around the trigonal axis and transforms to the $P\bar{1}$ triclinic symmetry at 190 K. In contrast to DMANaFe, the DMA^+ cations in DMAKCr remain disordered in the low temperature (LT) phase and exhibit a two-fold statistical type of disorder.[2] It has been suggested that such differences are due to smaller deformability of the KO_6 octahedra and that the phase transition in DMAKCr is exclusively driven by the reorientational motions of DMA^+ cations.[2]

Herein, the structural and high-pressure phonon properties of two heterometallic MOFs with the dimethylammonium cation (DMA^+), *i.e.* $[DMA]Na_{0.5}Cr_{0.5}(HCOO)_3$ (DMANaCr) and $[DMA]K_{0.5}Cr_{0.5}(HCOO)_3$ (DMAKCr) are reported. The DMA^+ cation is chosen due to its well-known properties in the perovskite-like MOFs with the framework composed of only one type of divalent metal ions.[9–21] These studies have revealed plenty of interesting phenomena depending on the metals building the metal-formate framework, including multiferroicity,[9–13,15] ferroelectricity,[19] pyroelectric,[21] magnetic[15,16,18] or dielectric[16,17] properties.

In the present study the dependencies how some properties can be tuned when divalent metal ions are substituted by a mixture of mono- and trivalent metal ions in the perovskite-type structure are explored. Therefore, high-pressure Raman studies of DMANaCr and DMAKCr are used to search for structural phase transitions and to better understand the structural properties responsible for the occurrence or lack of phase transition under different external stimuli. Our research are compared with the previously reported temperature behavior to get a full profile of structure–property relationships. Density functional theory calculations (DFT) are employed to obtain information on the energy of HBs and to understand changes related to the HBs during the experiment. Furthermore the magnitude of the vibrational entropy is calculated to understand how the structural dynamics affects the reorientational motions of the DMA^+ cation within the cage.

2. Experimental

2.1. Materials and instrumentation

All reagents (analytically grade) used for synthesis were commercially available and were used without further purification. The powder X-ray diffraction (XRD) patterns were obtained on an X'Pert PRO X-ray diffraction system equipped with a PIXcel ultrafast line detector, focusing mirror, and Soller slits for CuKα radiation (λ = 1.54056 Å). The high-pressure Raman spectra were recorded in back-scattering geometry using a microscope attached to a triple-grating spectrometer Jobin Yvon T64000. The 514.5 nm line of a solid-state ion laser was used as excitation and the spectral resolution was 2 cm^{-1}. In order to reach high pressures, a diamond anvil cell Diacell® μScopeDAC-RT(G) from Almax easyLab with a diamond of 0.4 mm of culets was used. The sample was loaded into a 100 μm hole drilled in a stainless steel gasket with a thickness of 200 μm using an electric discharge machine from Almax easyLab. The Nujol served as the pressure transmitting medium (PTM). Pressures were measured based on the shifts of the ruby R_1 and R_2 fluorescence lines. Raman spectra were fitted using Origin 2015 (64-bit) Sr2 version b9.2.272 (Academic) program. The parts of spectra were fitted with Lorentzian curves. The resulting standard errors of wavenumbers were smaller than 1 cm^{-1}.

2.2. Synthesis of the samples

The DMANaCr and DMAKCr crystals were synthesized using a hydrothermal technique described elsewhere.[1,2] The phase purity of both bulk samples was confirmed by the good match of their powder XRD patterns with a simulation from the single-crystal structural data (Fig. S1, ESI†) taken from crystal information files (CIF) available in literature.[1,2]

2.3. Quantum chemical calculations

Density functional theory (DFT) calculations are performed using the Vienna ab initio simulation package (VASP)[22] with PAW pseudopotentials and an energy cut-off of 700 eV. We use the PBEsol functional[23] with the D3 correction[24,25] to account for dispersive interactions. The atomic positions and unit cell dimensions are relaxed until all forces are below 0.01 eV $Å^{-1}$. Calculations are performed with a gamma-centred 2 × 2 × 1 *k*-point mesh for the DMANaCr and DMAZn unit cells which contain 6 cations and a 2 × 2 × 2 mesh for the smaller unit cell of DMAKCr in the LT phase, which contains only 4 cations. We do not perform calculations for the HT phase of DMAKCr, as optimisation of the unit cell shape leads to significant changes from that determined experimentally. This indicates that vibrations have a strong influence on the unit cell parameters, and thus they are poorly reproduced by standard DFT calculations, which concerns the electronic energy at 0 K only.

For structures containing Cr^{3+} ions the calculations are spin-polarised. We find an energy difference of less than 1 meV between the ferromagnetic and antiferromagnetic ordering of the Cr^{3+} ions in DMAKCr, showing a weak preference for arrangement of spins. We have chosen to optimise all the structures with ferromagnetic alignment of the spins on the Cr^{3+} ions.

Phonons are calculated using the finite displacement method, and the absence of imaginary frequencies at the Γ-point is used to confirm that the optimised structures represent local minima. We use Phonopy[26] to calculate the vibrational entropy as a function of temperature on a 5 × 5 × 5 *q*-point mesh. We furthermore calculate the site-projected phonon density of states, which can also be used to obtain the site-projected vibrational entropy, as previously described.[27]

The HB energy is calculated following the procedure described elsewhere.[4,28] The total electrostatic interaction is calculated as

the energy required to remove one cation from the unit cell, and the dominating monopole term is estimated as the energy required to remove a single atom cation (here Cs^+) from the same cage. Subtracting the monopole part of the electrostatic interaction from the total electrostatic interactions, the dipole and higher order terms remain, and these are assumed to be dominated by the HBs. Note that we use the same computational setup here as in previous works[4,28] and the calculated HB energies should thus be directly comparable.

3. Results and discussion

3.1. Crystal structure

DMANaCr and DMAKCr adopt perovskite-type metal-formate structures. Both crystallize in the trigonal $R\bar{3}$ symmetry (high-temperature phase, HT) and are isomorphic with other hetero-metallic MOFs; DMANaFe and AmNaCr.[1,2,4,7] The lattice constants and selected crystal parameters are listed in Tables S1 and S2 (ESI†).[1,2] The metal centres are octahedrally coordinated by the formate ions in the anti–anti mode configuration forming an infinite 3D network. Each Na^+ (K^+) ion has six Cr^{3+} ions as nearest metal neighbours and *vice versa*. The DMA^+ cations accommodated in the large cavities of the metal-formate framework are dynamically disordered into three equivalent positions, each being occupied with 1/3 probability.[1,2] Fig. 1 shows the thermally activated rotations of the DMA^+ cations around the trigonal axis in DMANaCr and DMAKCr. The previous vibrational and structural studies of DMANaCr showed that upon cooling the reorientational motions of the DMA^+ cations slow down.[1] In spite of this freezing the crystal does not undergo any structural phase transition down to 5 K.[1] In contrast to this behaviour, the DMAKCr crystal transforms at 190 K to the low temperature triclinic $P\bar{1}$ symmetry (LT phase, Fig. 1c). This structural phase transition is accompanied by the partial ordering of DMA^+ cations.[2] In the LT phase they statistically occupy two inequivalent positions with 0.55/0.45 probability ratio.[2]

In the HT $R\bar{3}$ phase the DMA^+ cations interact with the inorganic part *via* four N–H···O HBs (see Fig. 1 and Table S2, ESI†), two with NaO_6/KO_6 and two with CrO_6 octahedra. The N···O distances in DMANaCr range from 2.877 to 3.537 Å, with the two shorter bonds being to O_{Na}, and thus expected to be stronger than the other two bonds. The replacement of Na^+ by K^+ ions increases the N···O_{Cr} distances, while the N···$O_{Na/K}$ HBs remain almost unaffected. This behaviour suggests that the N–H···$O_{Na/K}$ HB is stronger than the N–H···O_{Cr} bond, thus the N–H···O_{Cr} HB is preferentially weakened in the larger DMAKCr formate framework.[1,2] This is further supported by the structure in the LT phase of DMAKCr, measured at 80 K. Here the most populated position of the molecule has two HBs with relatively short N–O distances (2.84 and 3.02 Å), both of which are created between DMA^+ cations and KO_6 octahedra.[2] The alternative molecular position only has one H-bond with an N–O_K distance of 2.89 Å.

3.2. DFT structure optimisation

Structural optimisation is performed using DFT calculations. The optimised unit cell parameters of the DMANaCr and DMAKCr compounds are compared with the experimental values and with the values obtained for the previously calculated DMAZn framework[28] in Table S1 (ESI†). The calculated unit cell and HB parameters are generally in good agreement with the experimental values, but with many HBs having larger angles than inferred from the H position assumed from the experimental data (Table S2, ESI†). We observe the same asymmetry of the formate anions as previously observed for AmNaCr[4] (Table S3, ESI†), where the C–$O_{Na/K}$ bonds are slightly shorter than the C–O_{Cr} bonds. This effect is caused by the more ionic character of the Na–O bonds compared with the Cr–O bonds, arising from the lower electronegativity of the Na^+ ions.

3.3. Pressure-dependent Raman spectra of DMANaCr

To better understand the stability of the studied MOFs under external stimuli we submitted DMANaCr and DMAKCr to high pressure conditions. Fig. 2 shows Raman spectra of DMANaCr measured up to 6.6 GPa and Fig. 3 shows the pressure-dependent evolution for the observed modes. The spectrum measured at ambient conditions is nearly the same as that obtained outside the pressure chamber, however some additional bands corresponding to the PTM are observed. The pressure-dependent behavior of the observed modes can be described

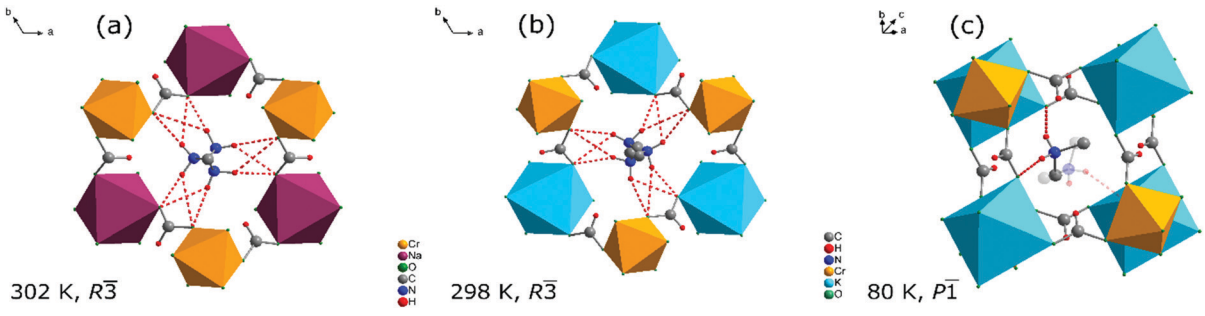

Fig. 1 DMA^+ cations anchored *via* H-bonding (red dashed lines) in the perovskite-like cavity in DMANaCr (a) and in DMAKCr for the HT (b) and LT (c) phases. At room temperature (a and b) DMA^+ cations are dynamically disordered into three equivalent positions, each occupied with 1/3 probability. In the triclinic structure (c) the DMA^+ cations are partially ordered into two non-equivalent positions occupied in a 0.55/0.45 ratio.[1,2] Hydrogens belonging to the methyl groups of the DMA^+ cations are omitted for clarity.

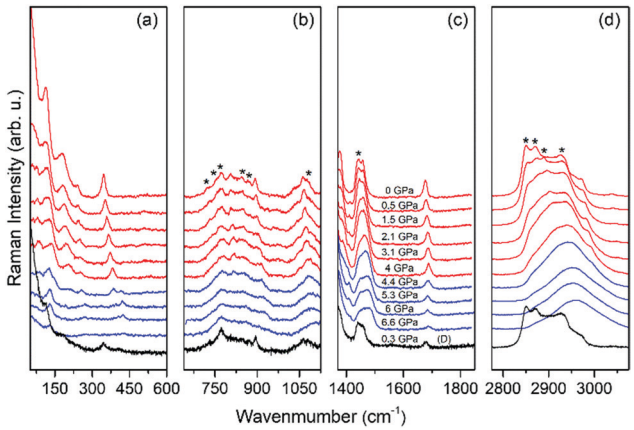

Fig. 2 The pressure-dependent Raman spectra of DMANaCr during compression and after decompression (*D*) in the 50–600 (a), 640–1125 (b), 1370–1850 (c), and 2775–3075 cm^{-1} (d) region. The stars denote the signal of the PTM.

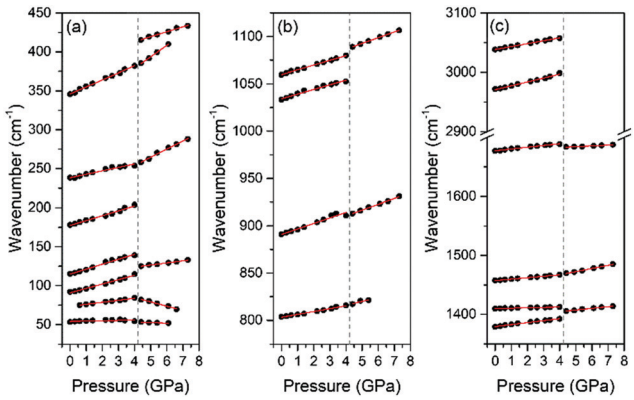

Fig. 3 The pressure-evolution of Raman bands for DMANaCr in (a) 25–450, (b) 775–1125 and (c) 1350–1700 together with 2900–3100 cm^{-1} ranges.

using a linear $\omega(P) = \omega_0 + \alpha P$ function describing interception at zero pressure (ω_0) and the vibrational pressure coefficient defined as $\alpha = d\omega/dP$. The results of fitting and the obtained parameters are summarized in Table 1. Fig. 2 and 3 show that qualitatively the spectra remain unchanged up to a pressure of 4.4 GPa. All observed modes exhibit an increase in wavenumber in this pressure range (Fig. 3 and Table 1). Especially pronounced hardening in the ambient-pressure (AP) phase equal to 8.98 cm^{-1} GPa^{-1} is observed for the translational $T'(Cr^{3+})$ mode near 350 cm^{-1} (no. 12). The α coefficient of the mode corresponding to $T'(Na^{+})$ is about 50% lower (4.42 cm^{-1} GPa^{-1}, no. 13) suggesting that the CrO_6 octahedra are strongly affected by the applied pressure, *i.e.* the compressibility of CrO_6 units is relatively large. Table 1 also shows that many of the observed modes corresponding to formate ions have large pressure coefficients ranging from 4.95 to 6.36 cm^{-1} GPa^{-1}. The values of α corresponding to the DMA^{+} and formate groups have similar values indicating that the whole crystal structure is affected when the pressure increases to 4 GPa.

A further increase in pressure to 4.4 GPa leads to some discontinuities in the observed wavenumber shifts and changes in the slope (α) of the wavenumber *vs.* pressure function. This behaviour indicates that DMANaCr undergoes a pressure-induced phase transition in the 4.0–4.4 GPa range. The disappearance of modes no. 1, 2, 6, 8, 14 and 16 and appearance of one new mode (no. 11) is a further proof of the occurring structural transformation. In the HP phase two of the α parameters corresponding to modes associated with translations of the Cr^{3+}, Na^{+} and $HCOO^{-}$ ions (no. 12 and 13) are very large (14.69 and 10.51 cm^{-1} GPa^{-1}, respectively), suggesting that the framework of the HP phase is still strongly affected by further increase of pressure. The spectrum after decompression is very similar to the spectrum recorded before the experiment. However, some bands belonging to the HP phase are observed, *i.e.* at about 388 cm^{-1} (mode no. 11) suggesting that the initial trigonal $R\bar{3}$ phase is not fully recovered.

The previous high pressure Raman studies of heterometallic MOFs with ammonium and imidazolium cations showed the presence of two phase transitions. The first one was observed at low pressures, at 0.5 GPa for AmNaCr and in the 0.4–1.1 GPa range for ImNaCr, whereas the second one occurred at 1.5 GPa and in the 3.2–4.0 GPa range, respectively.[4,5] It has been shown that in both cases the low-pressure transition is associated with the distortion of the framework and the transformation at higher pressures relates to the partial amorphization of the AmNaCr and ImNaCr samples.[4,5] In the case studied here, we observe only one phase transition for DMANaCr in the 4.0–4.4 GPa range. This transition most likely corresponds to the distortion of the metal formate framework accompanied by partial amorphization. This comparison let us draw the conclusion that the high-pressure stability of heterometallic MOFs depends on the templated cation following the trend $Am^{+} < Im^{+} < DMA^{+}$. The lack of the low-pressure phase transition for DMANaCr suggests that the flexibility of this metal-formate framework is lower compared to that of AmNaCr and ImNaCr.

The high-pressure effect on perovskite-like MOFs has been studied previously using Raman spectroscopy and X-ray diffraction for the $DMAM^{II}$ family (M^{II} = Cd,[29] Mg,[29] Mn,[30–32] Fe,[31] Cu,[31] Co,[33] and Ni[33]). Raman spectroscopy showed the presence of three phase transitions for DMAMg and DMAMn at 2.2 GPa, 4.0 GPa, and 5.6 GPa as well as at 2.1 GPa, 4.1 GPa, and 6.7 GPa, respectively, while only two phase transitions were found for DMACd, in the 1.2–2.0 GPa range and at 3.6 GPa. DMANi and DMACo exhibit only one phase transition in the 3–5 GPa range.[33] The two lowest transformations of DMAMg and DMAMn were assigned to the distortions of the metal-formate framework and the third one to the distortion of DMA^{+} cations.[29,30] Further Raman and IR studies suggest the presence of one phase transition for DMAMn initiated at about 3.4 GPa and completed at 6 GPa.[32] The high-pressure X-ray diffraction studies also indicated the presence of one phase transition for DMAMn, in the 5.5–5.6 GPa range resulting from the transformation from ambient-pressure trigonal $R\bar{3}c$ to triclinic $P1$ symmetry.[31] The absence of the remaining two transitions was explained by their character, *i.e.* it was assumed that they result from the change of local symmetry,[31] which would be better visible using vibrational methods.

As one can see, the modification of the transition metal-based framework to form the heterometallic framework composed of

Table 1 Raman zero wavenumbers (ω_0) for the two phases of DMANaCr and pressure coefficients (α) obtained from the linear fits on the data together with proposed assignment[a]

	AP-phase		HP-phase		
Mode no.	ω_0 (cm^{-1})	dω/dP (cm^{-1} GPa^{-1})	ω_0 (cm^{-1})	dω/dP (cm^{-1} GPa^{-1})	Assignment
1	3038.2 ± 0.2	4.96 ± 0.11			$\nu_{as}(CH_3)$
2	2970.9 ± 0.5	6.52 ± 0.20			$\nu_s(CH_3)$
3	1677.3 ± 0.3	3.02 ± 0.12	1677.7 ± 0.6	1.31 ± 0.10	$\nu_4(HCOO^-) + \delta(NH_2)$
4	1457.4 ± 0.1	2.41 ± 0.04	1445.9 ± 0.8	5.34 ± 0.13	$\delta_{as}(CH_3)$
5	1409.9 ± 0.1	0.64 ± 0.04	1393.2 ± 0.8	2.83 ± 0.13	$\delta_s(CH_3)$
6	1379.3 ± 0.3	3.35 ± 0.13			$\nu_5(HCOO^-)$
7	1059.9 ± 0.2	4.95 ± 0.08	1062.1 ± 0.4	6.10 ± 0.07	$\nu_6(HCOO^-)$
8	1034.3 ± 0.6	4.92 ± 0.25			$\nu_{as}(CNC)$
9	890.9 ± 0.9	5.84 ± 0.39	886.5 ± 1.3	6.03 ± 0.22	$\nu_s(CNC)$
10	803.2 ± 0.3	3.04 ± 0.11	799.7 ± 9.0	4.07 ± 1.83	$\nu_3(HCOO^-)$
11			387.7 ± 2.0	6.36 ± 0.34	$T'(Cr^{3+})$
12	346.2 ± 0.5	8.98 ± 0.20	320.1 ± 2.4	14.69 ± 0.46	$T'(Cr^{3+})$
13	238.3 ± 0.8	4.42 ± 0.33	212.1 ± 2.5	10.51 ± 0.42	$T'(Na^+) + T(HCOO^-)$
14	177.3 ± 0.6	6.24 ± 0.27			$L(HCOO^-)$
15	114.7 ± 0.5	6.36 ± 0.23	113.0 ± 0.7	2.69 ± 0.12	$L(HCOO^-)$
16	90.7 ± 0.4	5.64 ± 0.19			$T'(DMA^+) + L(HCOO^-)$
17	73.0 ± 0.3	2.57 ± 0.10	106.7 ± 2.3	−5.53 ± 0.41	$T'(DMA^+) + L(HCOO^-)$
18	53.9 ± 0.5	0.41 ± 0.20	56.8 ± 1.1	−0.86 ± 0.21	$T'(DMA^+) + L(HCOO^-)$

[a] Key: ν_s, ν_{as}, δ_s, δ_{as}, ν_4, ν_5, ν_6, T′ and L denote symmetrical stretching, antisymmetric stretching, symmetric bending, antisymmetric bending, the antisymmetric CO stretching, the CH in-plane bending, the CH out-of-plane bending, translational and librational mode.

Na^+ and Cr^{3+} ions leads to changes in its stability and flexibility. The stability (resistance to the high-pressure conditions) depends on the templated cation. For the smallest Am^+ cation the transition from a zinc-formate framework (AmZn) to a heterometallic-formate framework (AmNaCr) decreases the pressure of the phase transition from the 0.94–1.35 GPa[34] range to about 0.5 GPa suggesting a weak destabilization. Similar behaviour was observed for ImMg in comparison to ImNaCr that undergo phase transitions at 3 GPa[35] and in the 0.4–1.1 GPa range, respectively. For the DMA^+ cation the comparison is more complicated, since DMANaCr only has one phase transition while the Mg, Mn and Cd based compounds have several. The pressure of the last phase transition, which corresponds to the amorphization of the structures, is higher in both the DMAMg and DMAMn compounds than in DMANaCr, but slightly lower for DMACd.[29–31]

To compare the flexibility (deformation ability) of heterometallic MOFs and divalent-formate frameworks the following factors should be taken into account; the pressure of phase transition(s), the number of transitions, the pressure of amorphization and the values of the pressure coefficients (α). The first three factors suggest that the structures of AmNaCr and ImNaCr are more flexible when compared to their divalent-metal analogues. The situation is less clear for DMANaCr which has fewer phase transitions than the divalent analogues, but a lower amorphization pressure than both DMAMn and DMAMg. Overall, however, the low pressure of amorphization observed for all three heterometallic analogues and their relatively higher pressure coefficients suggest that the heterometallic perovskites have more flexible structures compared with the divalent-metal analogues.

3.4. Pressure-dependent Raman spectra of DMAKCr

To understand the effect of K^+ ions on the high-pressure behaviour of heterometallic perovskites, we carried out our experiment for another analogue, DMAKCr. Fig. 4 presents high-pressure Raman spectra at selected pressures up to 4.7 GPa and Fig. 5 shows the pressure-evolution of observed bands. Table 2 lists the fitting parameters together with proposed assignments.

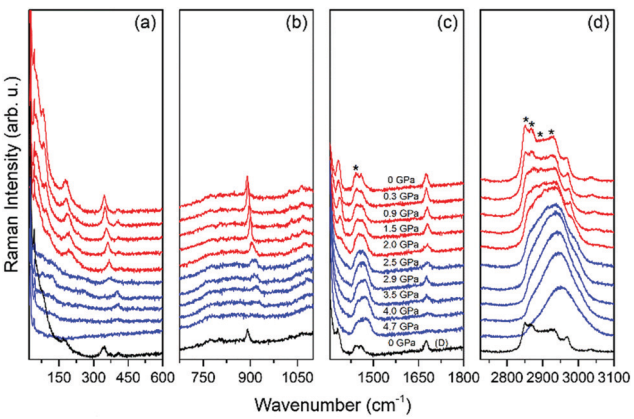

Fig. 4 The pressure-dependent Raman spectra of DMAKCr during compression and after decompression (D) in the 50–600 (a), 675–1100 (b), 1355–1800 (c), and 2725–3100 cm^{-1} (d) region. The stars denote the signal of the PTM.

The obtained results show that the high-pressure behaviour of DMAKCr is very similar to that of DMANaCr. In the ambient pressure (AP) phase all observed modes exhibit an increase in wavenumber up to 2 GPa. The strongest hardening is observed for modes corresponding to the metal-formate framework and DMA^+ cations as it was observed for DMANaCr. However, the structural phase transition in DMAKCr occurs in the 2.0–2.5 GPa range, at much lower pressure than for DMANaCr. The observed features in the spectra are very similar for both compounds, suggesting that this phase transition has the same nature and

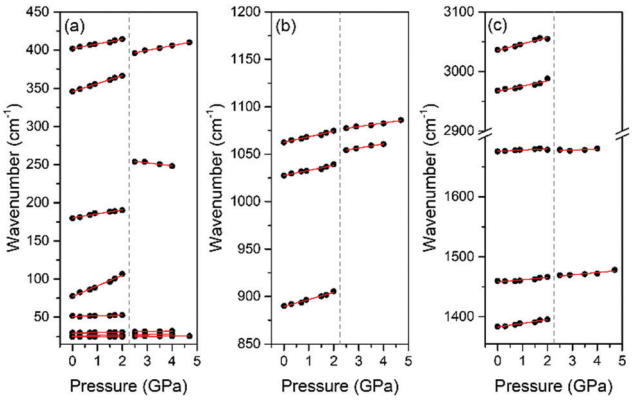

Fig. 5 The pressure-evolution of Raman bands for DMAKCr in (a) 15–450, (b) 850–1200 and (c) 1355–1700 together with 2900–3100 cm^{-1} ranges.

involves the same structural changes. In particular, one can notice the rise of a band at about 380 cm^{-1} in the HP phase. The significant difference is that the α coefficient for mode no. 11′ of DMAKCr is negative. This pronounced softening under pressure reveals that contributions from anharmonicity become important and points to some crystal instabilities.[34,36] Similar behaviour was previously observed for AmNaCr and ImNaCr perovskites.[4,5]

Our high-pressure Raman scattering experiment shows that replacement of the Na^+ ions in the metal-formate heterometallic framework by larger K^+ ions leads to a decrease in stability observed as a decrease of the pressure at which the phase transition occurs. Our previous temperature-dependent studies of DMANaCr and DMAKCr showed that the temperature-induced order–disorder phase transition is observed exclusively for DMAKCr at 190 K.[1,2] It was assumed that the temperature-induced phase transition in DMAKCr involves a weak distortion (more likely tilting of octahedra) of the framework. It was suggested that this distortion occurred as a result of the lower deformability of the KO_6 octahedra compared to the NaO_6 ones,[2] however our present study shows that the flexibility of the DMAKCr compound is higher than for DMANaCr. We suppose that the previously observed weak distortion of the framework associated with the order–disorder phase transition does not result from the lower deformability of KO_6 but can be attributed to the presence of larger voids accommodating the DMA^+ cations, implying that they have more space for reorientations.

3.5. Phase transitions, hydrogen bonding and structural flexibility

Based on the DFT optimised structures we now try to pinpoint the structural properties that lead to the existence of a phase transition in DMAKCr[2] and DMAZn[28] but not in in DMANaCr.[1] The strength of the HBs, the difference in vibrational entropy between phases and the ability of the framework to deform (its flexibility) are some of the factors that have previously been suggested to influence the existence of phase transitions.[1–4,6,7,27,28,37,38] We have therefore investigated these properties for the two heterometallic compounds, DMANaCr and DMAKCr, as well as the corresponding Zn^{2+}-based compound, DMAZn.

The calculated total HB energy (E_{tot}) and energy per N–H bond (E_{N-H}) are given in Table 3, along with the phase transition temperatures (T_C), the calculated volumes per cation (V_{cation}) and the tolerance factors (TF).[39] Our calculations show that the total HB energy follows the trend DMAKCr > DMANaCr > DMAZn, however all three values are relatively low compared to previous calculations for different cations.[4,28] This is not surprising, since DMA^+ only has two N–H bonds to form hydrogen bonds with, and we previously showed that the total HB energy correlates with the number of N–H bonds in the molecule. The room-temperature experimental XRD and vibrational data indicate that the geometries of the H-bonding in the RT phases of DMANaCr and DMAKCr are very similar,[1,2] however the calculations show that the total HB energy for DMAKCr (0.62 eV) is higher than for DMANaCr (0.48 eV). This is probably

Table 2 Raman zero wavenumbers (ω_0) for the two phases of DMAKCr, pressure coefficients (α) obtained from the linear fits on the data together with proposed assignment[a]

	AP-phase		HP-phase		
Mode no.	ω_0 (cm^{-1})	dω/dP (cm^{-1} GPa^{-1})	ω_0 (cm^{-1})	dω/dP (cm^{-1} GPa^{-1})	Assignment
1′	3035.3 ± 1.2	10.98 ± 0.95			$\nu_{as}(CH_3)$
2′	2967.1 ± 1.7	8.64 ± 1.36			$\nu_s(CH_3)$
3′	1675.8 ± 0.7	2.12 ± 0.56	1672.9 ± 4.7	1.66 ± 1.44	$\nu_4(HCOO^-) + \delta(NH_2)$
4′	1458.2 ± 0.9	3.56 ± 0.72	1458.2 ± 3.5	3.89 ± 0.96	$\delta_{as}(CH_3)$
5′	1382.7 ± 0.6	6.24 ± 0.53			$\nu_5(HCOO^-)$
6′	1062.5 ± 0.4	5.87 ± 0.35	1068.1 ± 1.0	3.72 ± 0.28	$\nu_6(HCOO^-)$
7′	1027.6 ± 0.5	5.34 ± 0.43	1043.5 ± 1.0	4.33 ± 0.30	$\nu_{as}(CNC)$
8′	889.4 ± 0.6	7.45 ± 0.46			$\nu_s(CNC)$
9′	401.9 ± 0.4	6.08 ± 0.31			$\delta(CNC)$
10′	345.9 ± 0.2	10.34 ± 0.17	380.6 ± 1.1	6.27 ± 0.32	$T'(Cr^{3+})$
11′			264.1 ± 2.5	−3.96 ± 0.76	$\tau(NH_2) + \tau(CH_3) + T'(K^+)$
12′	180.3 ± 0.6	5.29 ± 0.47			$L(HCOO^-) + T'(K^+)$
13′	77.2 ± 1.0	13.85 ± 0.78			$T'(DMA^+)$
14′	50.8 ± 0.3	0.85 ± 0.27			$T'(DMA^+) + T'(HCOO^-)$
15′	29.3 ± 0.0	0.49 ± 0.03	29.2 ± 0.3	0.62 ± 0.09	$T'(HCOO^-)$
16′	25.9 ± 0.0	0.47 ± 0.03	26.3 ± 0.2	0.36 ± 0.07	$T'(HCOO^-)$
17′	24.4 ± 0.0	0.15 ± 0.02	24.8 ± 0.2	0.12 ± 0.04	$T'(HCOO^-)$

[a] Key: ν_s, ν_{as}, δ_s, δ_{as}, ν_4, ν_5, ν_6, T′ and L denote symmetrical stretching, antisymmetric stretching, symmetric bending, antisymmetric bending, the antisymmetric CO stretching, the CH in-plane bending, the CH out-of-plane bending, translational and librational mode.

Table 3 The hydrogen bonding energies (E_{tot}) and energy per N–H bond in the cation (E_{N-H}) for the two DMA^+-based heterometallic perovskites and the previously calculated Zn^{2+}-based compound. We also give the volume per cation (V_{cation}) and the tolerance factor (TF), calculated as described previously[35]

	DMANaCr	DMAKCr	DMAZn[24]
E_{tot} (eV)	0.48	0.62	0.36
E_{N-H} (eV)	0.24	0.31	0.18
T_C (K)	—	190[2]	156
V_{cation} (Å^3)	218	241	206
TF	0.95	0.89	0.94

because the HB energy of DMAKCr is calculated for the LT-phase, which has a different HB arrangement with all HBs involving the KO_6 octahedral unit, whereas in DMANaCr and the HT phase of DMAKCr the HBs involve both the NaO_6 and CrO_6 octahedral units. The higher E_{tot} in DMAKCr thus reflects that the HBs bounded to the KO_6 octahedra (see Table S2, ESI†) are stronger than the alternative bonds to CrO_6 octahedra. The preference for HBs to $O_{Na/K}$ arises because of the low electronegativity of the alkali metals (0.9 and 0.8 for Na and K, respectively) compared to chromium (1.7), which would lead to a more ionic metal–oxygen bond (Table S3, ESI†). Therefore, the oxygen anion at the Na^+/K^+ end is more negative leading to a stronger hydrogen bond. This also explains why the total HB energy in DMAZn is generally lower (0.36 eV) than in the mixed metal systems, since zinc has an electronegativity of 1.7 and thus a less ionic Zn–O bond.

While the calculated HB energy is higher for DMAKCr (Table 3), a smaller value of the TF (0.89) and high V_{cation} indicate that there is more space for the templated organic cation to reorient. The calculated TFs of DMANaCr and DMAZn are similar (0.95 and 0.94, respectively), however the much lower HB energy of the latter could explain why a phase transition is observed in this compound but not in DMANaCr.

Another thing that can affect the ability of the cations to reorient is the flexibility of the metal formate cage. This feature can be characterised by the phonon frequencies of the cage and the vibrational entropy, which is dominated by the low frequency modes that are populated at RT. The phonon frequencies depend on the relation between the force constant of the bonds and the reduced mass of the involved atoms. The reduced mass increases following the series NaCr < KCr < Zn, which would lead to an expected ordering of the frequencies Zn < KCr < NaCr, however the Cr–O bond is expected to be significantly stronger (more covalent and shorter) than the other bonds, shifting it towards higher frequencies. The combined effect of these two factors can be seen by looking at the phonon density of states (pdos) projected on the respective metal sites (Fig. 6). It is clearly seen that Cr atoms give contributions at much higher frequencies than the other metals, while contributions from the K atoms are found at the very low frequencies.

In general, the vibrational entropy of DMAKCr is higher at all temperatures as seen in Fig. 7 and Table 4. The vibrational entropy can be projected on the DMA^+ molecule (S_{vib}^{mol}) and the cage (S_{vib}^{cage}),[27] and the results from this analysis show that the

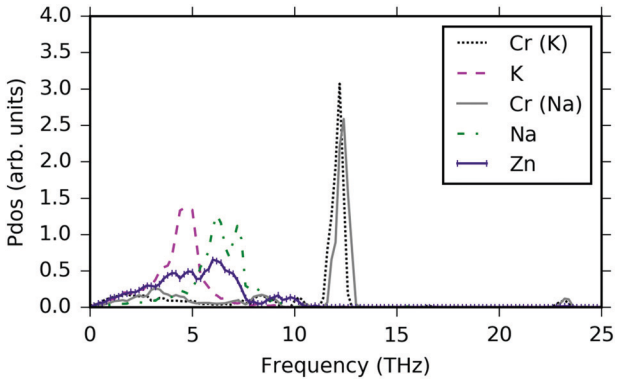

Fig. 6 Phonon projected density of states for DMANaCr, DMAKCr and DMAZn. Each curve is normalised by the number of atoms of this type.

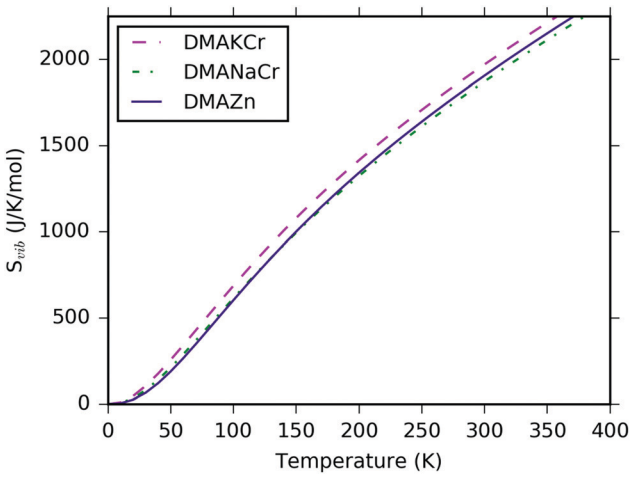

Fig. 7 Vibrational entropy (S_{vib}) as a function of temperature for DMANaCr, DMAKCr and DMAZn. The curves are per unit containing 4 cations.

DMAKCr analogue has a larger vibrational entropy for both the DMA^+ cation and the cage compared with the DMANaCr and DMAZn compounds. The higher entropy can be explained by the lower frequencies associated with the heavier K^+ ions compared with Na^+ ions, and the lower TF, which implies that there is more space for the DMA^+ molecules to move in the K-based structure. The results thus indicate that the DMAKCr compound is the most flexible of the three structures, giving another plausible explanation for the occurrence of a structural phase transition in DMAKCr. We note that the calculations described above are done for the LT phase of DMAKCr. The HT phase, which is in the same space group as the DMAZn and DMANaCr compounds, is likely to have a lower HB energy, since the HBs are no longer exclusively to the KO_6 octahedra. This loss in energy must be compensated by a higher entropy in order to drive the phase transition.

3.6. DFT simulation of high pressure

To gain further insight into the effect of an applied pressure we calculated the bulk modulus for all three structures. This is done by optimising the structures at a number of different

Table 4 Site-projected vibrational entropy (S_{vib}) at 150 K for DMANaCr, DMAKCr and DMAZn (*i.e.* below the transition temperatures of all materials). The values are per unit containing 4 cations[a]

	DMANaCr	DMAKCr	DMAZn[24]
S_{vib} (J mol^{-1} K^{-1})	663	718	667
S_{vib}^{mol} (J mol^{-1} K^{-1})	214	235	224
S_{vib}^{cage} (J mol^{-1} K^{-1})	450	483	443

[a] Key: S_{vib}^{mol} and S_{vib}^{cage} denote molecule- and cage-projected entropy.

volumes and fitting the resulting energy *vs.* volume to an equation of state. We find values of 17 GPa (LT phase of DMAKCr), 21 GPa (DMANaCr) and 30 GPa (DMAZn) for the three compounds, which follows the expected order of stability under pressure.

For DMANaCr, where the DFT optimised structure is identical with the RT experimental structure, we furthermore investigated the structural effects of an applied pressure. We consider the structure optimised at a fixed volume of 1253 Å^3.

This volume corresponds to 96% of the DFT optimised volume, and from the calculated cell stress this is equivalent to an external pressure of about 1 GPa. The relative lengths of the unit cell vectors were allowed to change during the optimisation, resulting in a larger relative contraction of the *c* vector (about 3%) compared with the *a* and *b* vectors (about 0.5%). This is similar to the behaviour observed by XRD for the divalent-metal DMA$^+$ frameworks based on Fe^{2+} and Mn^{2+} ions.[31] The DFT analysis shows that the HBs are only slightly compressed, *i.e.* the H$\cdots$O$_{Cr}$ distances decrease from 1.89–1.92 Å to 1.85–1.87 Å (Table S4, ESI†) and the shorter H$\cdots$O$_{Na}$ bond remains at almost the same length shrinking from 1.62 Å to 1.60–1.61 Å. It is worth noticing that similar pressure-dependent DFT calculations performed previously for AmNaCr also showed the strongest contraction in the *c* axis and a minimal shortening of the short HBs.[4] This suggests that short H-bonds have a strong influence on the structural behaviour under pressure, preventing compression in the bonding direction.

4. Conclusions

We have investigated heterometallic MOFs templated by the DMA$^+$ cation crystallizing in the perovskite-type architecture, DMANaCr and DMAKCr, and compared with previous results for DMAZn. We performed DFT calculations to optimise their structures, model their properties and relate these to the existence of phase transitions upon heating or applied pressure.

The calculated strength of the HBs between the DMA$^+$ cation and the metal-formate cage follows the trend DMZn < DMANaCr < DMAKCr. This suggests that HBs to O$_{Na/K}$ are stronger than HBs to O$_{Cr}$ and O$_{Zn}$, following the degree of ionicity in the metal–oxygen bond.

A smaller value of the tolerance factor for DMAKCr indicates that there is more space for the DMA$^+$ cation to move, and this correlates with a higher vibrational entropy than in the DMANaCr and DMAZn compounds. DMAKCr thus has a more flexible crystal structure, and this leads to the occurrence of an order–disorder phase transition at 190 K and a pressure induced transition in the 2.0–2.5 GPa range. Raman study of this phase transition confirms that it involves strong deformations of the metal-formate framework, especially pronounced for the subnetwork of CrO_6 octahedra and the DMA$^+$ cations, and that it is not fully reversible. A pressure-induced phase transition with a similar mechanism occurs in the 4.0–4.4 GPa range in DMANaCr. The higher transition pressure and the absence of a thermally induced phase transition correlates with the higher value of the TF (less space for the cation to move) together with the relatively strong HBs in this compound. Finally, DMAZn has a similar TF to DMANaCr, however the significantly lower HB energy could be the reason that a temperature-induced phase transition is still observed at 156 K. The pressure-response of the DMAZn compound is not known, but the amorphization pressure of other divalent-metal based DMA formate frameworks has been found to be slightly higher than for the DMANaCr and DMAKCr compounds studied here. Together, our results illustrate how the subtle balance between structural properties such as hydrogen bonding and molecular vibrations can influence macroscopic physical phenomena, *i.e.* phase transitions under external stimuli.

Conflicts of interest

There are no conflicts to declare.

Acknowledgements

This research was supported by the National Science Centre (NCN) in Poland under project no. DEC-2015/17/D/ST5/01339. K. L. S. and A. W. are funded by ERC programme grant no. 277757 and the Royal Society. The authors acknowledge computing support from the UK national supercomputing service (Archer), *via* membership of UK Materials Chemistry Consortium which is funded by EPSRC (EP/L000202).

References

1 M. Mączka, B. Bondzior, P. Dereń, A. Sieradzki, J. Trzmiel, A. Pietraszko and J. Hanuza, *Dalton Trans.*, 2015, **44**, 6871–6879.
2 M. Ptak, A. Gągor, A. Sieradzki, B. Bondzior, P. Dereń, A. Ciupa, M. Trzebiatowska and M. Mączka, *Phys. Chem. Chem. Phys.*, 2017, **19**, 12156–12166.
3 M. Ptak, M. Mączka, A. Gągor, A. Sieradzki, B. Bondzior, P. Dereń and S. Pawlus, *Phys. Chem. Chem. Phys.*, 2016, **18**, 29629–29640.
4 M. Ptak, D. Stefańska, A. Gągor, K. L. Svane, A. Walsh and W. Paraguassu, *Phys. Chem. Chem. Phys.*, 2018, **2**, 22284–22295.
5 M. Ptak, B. Zarychta, D. Stefańska, A. Ciupa and W. Paraguassu, *Dalton Trans.*, 2019, **48**, 242–252.
6 M. Ptak, M. M. Mączka, A. Gągor, A. Sieradzki, A. Stroppa, D. Di Sante, J. M. Perez-Mato and L. Macalik, *Dalton Trans.*, 2016, **45**, 2574–2583.
7 M. Mączka, A. Pietraszko, L. Macalik, A. Sieradzki, J. Trzmiel and A. Pikul, *Dalton Trans.*, 2014, **43**, 17075–17084.

8 Y. Yu, R. Shang, S. Chen, B.-W. Wang, Z.-M. Wang and S. Gao, *Chem. – Eur. J.*, 2017, **23**, 9857–9871.
9 P. Jain, V. Ramachandran, R. J. Clark, H. D. Zhou, B. H. Toby, N. S. Dalal, H. W. Kroto and A. K. Cheetham, *J. Am. Chem. Soc.*, 2009, **131**, 13625–13627.
10 D.-W. Fu, W. Zhang, H.-L. Cai, Y. Zhang, J.-Z. Ge, R.-G. Xiong, S. D. Huang and T. Nakamura, *Angew. Chem., Int. Ed.*, 2011, **50**, 11947–11951.
11 Y. Tian, A. Stroppa, Y. Chai, L. Yan, S. Wang, P. Barone, S. Picozzi and Y. Sun, *Sci. Rep.*, 2015, **4**, 6062.
12 Y. Tian, S. Shen, J. Cong, L. Yan, S. Wang and Y. Sun, *J. Am. Chem. Soc.*, 2016, **138**, 782–785.
13 W. Wang, L.-Q. Yan, J.-Z. Cong, Y.-L. Zhao, F. Wang, S.-P. Shen, T. Zou, D. Zhang, S.-G. Wang, X.-F. Han and Y. Sun, *Sci. Rep.*, 2013, **3**, 2024.
14 P. Jain, N. S. Dalal, B. H. Toby, H. W. Kroto and A. K. Cheetham, *J. Am. Chem. Soc.*, 2008, **130**, 10450–10451.
15 M. Mączka, A. Gągor, B. Macalik, A. Pikul, M. Ptak and J. Hanuza, *Inorg. Chem.*, 2014, **53**, 457–467.
16 N. Abhyankar, M. Lee, M. Foley, E. S. Choi, G. Strouse, H. W. Kroto and N. S. Dalal, *Phys. Status Solidi RRL*, 2016, **10**, 600–605.
17 M. Sánchez-Andújar, S. Presedo, S. Yáñez-Vilar, S. Castro-García, J. Shamir and M. A. Señarís-Rodríguez, *Inorg. Chem.*, 2010, **49**, 1510–1516.
18 M. Šimenas, M. Ptak, A. H. Khan, L. Dagys, V. Balevičius, M. Bertmer, G. Völkel, M. Maczka, A. Pöppl and J. Banys, *J. Phys. Chem. C*, 2018, **122**, 10284–10292.
19 P. Jain, A. Stroppa, D. Nabok, A. Marino, A. Rubano, D. Paparo, M. Matsubara, H. Nakotte, M. Fiebig, S. Picozzi, E. S. Choi, A. K. Cheetham, C. Draxl, N. S. Dalal and V. S. Zapf, *npj Quantum Mater.*, 2016, **1**, 16012.
20 M. Mączka, M. Ptak and L. Macalik, *Vib. Spectrosc.*, 2014, **71**, 98–104.
21 Y. Ma, J. Cong, Y. Chai, L. Yan, D. Shang and Y. Sun, *Appl. Phys. Lett.*, 2017, **111**, 042901.
22 G. Kresse and J. Hafner, *Phys. Rev. B: Condens. Matter Mater. Phys.*, 1993, **47**, 558–561.
23 J. P. Perdew, A. Ruzsinszky, G. I. Csonka, O. A. Vydrov, G. E. Scuseria, L. A. Constantin, X. Zhou and K. Burke, *Phys. Rev. Lett.*, 2008, **100**, 136406.
24 S. Grimme, J. Antony, S. Ehrlich and H. Krieg, *J. Chem. Phys.*, 2010, **132**, 154104.
25 S. Grimme, S. Ehrlich and L. Goerigk, *J. Comput. Chem.*, 2011, **32**, 1456–1465.
26 A. Togo and I. Tanaka, *Scr. Mater.*, 2015, **108**, 1–5.
27 K. T. Butler, K. Svane, G. Kieslich, A. K. Cheetham and A. Walsh, *Phys. Rev. B*, 2016, **94**, 180103.
28 K. L. Svane, A. C. Forse, C. P. Grey, G. Kieslich, A. K. Cheetham, A. Walsh and K. T. Butler, *J. Phys. Chem. Lett.*, 2017, **8**, 6154–6159.
29 M. MącZka, T. Almeida da Silva, W. Paraguassu and K. Pereira Da Silva, *Spectrochim. Acta, Part A*, 2016, **156**, 112–117.
30 L. Xin, Z. Fan, G. Li, M. Zhang, Y. Han, J. Wang, K. P. Ong, L. Qin, Y. Zheng and X. Lou, *New J. Chem.*, 2016, **41**, 151–159.
31 I. E. Collings, M. Bykov, E. Bykova, M. Hanfland, S. Van Smaalen, L. Dubrovinsky and N. Dubrovinskaia, *CrystEngComm*, 2018, **20**, 3512–3521.
32 A. V. Chitnis, H. Bhatt, M. Maczka, M. N. Deo and N. Garg, *Dalton Trans.*, 2018, **47**, 12993–13005.
33 S. Sobczak, A. Chitnis, M. Andrzejewski, M. Maczka, S. Gohil, N. Garg and A. Katrusiak, *CrystEngComm*, 2018, **20**, 5348–5355.
34 M. Mączka, P. Kadłubański, P. T. C. Freire, B. Macalik, W. Paraguassu, K. Hermanowicz and J. Hanuza, *Inorg. Chem.*, 2014, **53**, 9615–9624.
35 M. Mączka, N. L. Marinho Costa, A. Gągor, W. Paraguassu, A. Sieradzki and J. Hanuza, *Phys. Chem. Chem. Phys.*, 2016, **18**, 13993–14000.
36 M. Maczka, A. G. Souza Filho, W. Paraguassu, P. T. C. Freire, J. Mendes Filho and J. Hanuza, *Prog. Mater. Sci.*, 2012, **57**, 1335–1381.
37 G. Kieslich, S. Kumagai, K. T. Butler, T. Okamura, C. H. Hendon, S. Sun, M. Yamashita, A. Walsh and A. K. Cheetham, *Chem. Commun.*, 2015, **51**, 15538–15541.
38 M. Mączka, A. Gągor, M. Ptak, W. Paraguassu, T. A. Da Silva, A. Sieradzki and A. Pikul, *Chem. Mater.*, 2017, **29**, 2264–2275.
39 G. Kieslich, S. Sun and A. K. Cheetham, *Chem. Sci.*, 2014, **5**, 4712–4715.

